Electronic Supplementary Material (ESI) for Inorganic Chemistry Frontiers.

An Excellent Lead Oxyiodide with Strong Second-Harmonic Generation Response and Large Birefringence Induced by the Oriented Arrangement of Highly Distorted [PbO_4I_2] Polyhedrons

Zi-Qi Zhou,[a] Rui-Biao Fu,*[a,b] Hong-Xin Tang,[a] Zu-Ju Ma,*[c] and Xin-Tao Wu[a]

[a] State Key Laboratory of Structural Chemistry, Fujian Institute of Research on the Structure of Matter, Chinese Academy of Sciences, Fuzhou, Fujian 350002, P. R. China.
[b] Fujian Science & Technology Innovation Laboratory for Optoelectronic Information of China, Fuzhou, Fujian 350108.
[c] School of Environmental and Materials Engineering, Yantai University, Yantai, 264005, P. R. China.

Table of Contents

1. Experimental Procedures

Reagents.

Lead oxide (PbO, 98%) and cesium carbonate (Cs_2CO_3, 98%) were purchased from Aladdin Chemical Industry Co. Ltd. Potassium iodide (KI, 99%), potassium carbonate (K_2CO_3, 99%), malonic acid (99%) and ethanol (EtOH, 98%) were obtained from Sinopharm Reagent and used as received.

Synthesis.

Single crystals of **KPMI** and **CPMI** were obtained by a solvothermal method. For **CPMI**, a mixture of 0.325 g Cs_2CO_3 (1 mmol), 0.223 g PbO (1 mmol), 0.520 g CsI (2 mmol), 0.104 g malonic acid (1 mmol) and 2 mL EtOH was added into 23 mL Teflon-lined stainless-steel autoclaves and heated at 100 ^oC for 7 days and gradually cooled to room temperature with a rate of 3 $^oC \cdot h^{-1}$. The products were washed by ethanol. Crystals of **CPMI** were obtained in ca. 52% yield based on PbO. For **KPMI**, a hybrid of 0.158 g K_2CO_3 (1 mmol), 0.223 g PbO (1 mmol), 0.332 g KI (2 mmol), 0.104 g malonic acid (1 mmol) and 2 mL EtOH was added into 23 mL Teflon-lined stainless-steel autoclaves, then heated at 120 ^oC for 7 days and gradually cooled to room temperature with a rate of 3 $^oC \cdot h^{-1}$. The products were washed by ethanol. Crystals of **KPMI** were obtained in ca. 17% yield based on PbO.

Single-Crystal X-ray Diffraction.

Single-crystal X-ray diffraction data of **CPMI** and **KPMI** were collected on a Rigaku Saturn 724 CCD diffractometer equipped with a graphite-monochromated Mo Kα radiation. The data reduction was integrated with the program Crystal Clear version 1.30. Their structures were solved with a direct method by using the SHELXT and refined by the SHELXL full-matrix least-squares program.[1-2] Their structures were checked by the PLATON and no higher symmetries were suggested.[3] CCDC 2156743 for **CPMI** and 2156749 for **KPMI**. The details of crystal data can be acquired free of charge via www.ccdc.cam.ac.uk/data_request/cif.

Powder X-ray Diffraction.

Powder XRD measurement for **KPMI** was performed by using a Rigaku Miniflex 600 diffractometer with Cu Kα radiation (λ =1.540598 Å) at room temperature. The data were obtained in the 2θ range of 5-55° with a step width of 0.02°.

Thermal Analysis.

Thermogravimetric analysis (TGA) of **KPMI** was performed on a NETZCH STA 449F3

thermal analysis instrument at a heating rate of 10 $^{o}C \cdot min^{-1}$ in a flowing nitrogen atmosphere from 30 to 800 ^{o}C.

Elemental Analysis.

Elemental analysis of **KPMI** were performed using a field emission scanning electron microscope (FESEM, JSM6700F) with an energy dispersive X-ray spectroscope (EDS, Oxford INCA). EDS confirms the presences of K, Pb, I, C and O elements. The molar ratio of K: Pb: I of 1.95: 1: 2.07 is in good agreement with the calculated value of 2:1:2 based on single-crystal X-ray diffraction data. C and H analyses were carried out with a Vario EL III element analyzer. Anal. Calcd. for **KPMI**: C 5.61, H 0.31 %. Found: C 4.97, H <=0.30 %.

UV–Vis–NIR Diffuse Reflectance Spectroscopy.

UV–vis–NIR diffuse reflectance spectrum was recorded in the wavelength range of 190-2500 nm at room temperature on a PrkinElmer Lambda 950 ultraviolet/visible/near-infrared spectrophotometer using $BaSO_4$ as the standard reference. The reflection spectrum was converted into the absorption spectrum by using the Kubelka-Munk function.[4]

IR Spectroscopy.

IR spectrum from 400 to 4000 cm^{-1} was performed at room temperature on a VERTEX70 FT-IR spectrometer instrument using Attenuated Total Reflectance (ATR) method. The crystal sample was tightly fitted to the total reflection crystal. In FT-IR spectrum of **KPMI**, two absorption bands at 1546 cm^{-1} and 1420 cm^{-1} are attributed to the antisymmetric stretching vibration and stretching vibration of the carboxylate group, respectively (**Fig. S11**). The bending deformation vibration of -CH_2 is observed at 1340 cm^{-1}.

SHG Test.

Powder SHG measurement was carried out on a pulsed Q-switched Nd:YAG solid-state laser using the Kurtz-Perry method under a wavelength of 1064 nm laser at room temperature.[5] Crystalline samples and microcrystalline KDP as the reference were ground and sieved into progressively increasing particle size ranges: 25-45, 45-75, 75-109, 109-150 and 150-212 μm.

Computational Details.

Our DFT calculations have been performed using the Vienna ab initio simulation package (VASP)[6-8] with the Perdew-Burke-Ernzerhof (PBE)[9] exchange correlation functional. The projected augmented wave (PAW) potentials have been used to treat the ion-electron interactions.[10] A Γ-centered 7×7×3 Monkhorst-Pack grid for the Brillouin zone sampling[11] and a cutoff energy of 500 eV for the plane wave expansion were found to get convergent lattice parameters and self-consistent energies. The electronic structures and electron localization

function (ELF) plots displayed in this work were visualized by Device Studio [12] and VESTA.[13]

In calculation of the static $\chi^{(2)}$ coefficients, the so-called length-gauge formalism derived by Aversa and Sipe[14] and modified by Rashkeev *et al*[15] is adopted, which has been proved to be successful in calculating the second order susceptibility for semiconductors and insulators.[16-19] In the static case, the imaginary part of the static second-order optical susceptibility can be expressed as:

$$\chi^{abc} = \frac{e^3}{\hbar^2\Omega}\sum_{nml,k}\frac{r^{a}_{nm}(r^{b}_{ml}r^{c}_{ln}+r^{c}_{ml}r^{b}_{ln})}{2\omega_{nm}\omega_{ml}\omega_{ln}}[\omega_n f_{ml}+\omega_m f_{ln}+\omega_l f_{nm}]$$

$$+\frac{ie^3}{4\hbar^2\Omega}\sum_{nm,k}\frac{f_{nm}}{\omega^{2}_{mn}}[r^{a}_{nm}(r^{b}_{mn;c}+r^{c}_{mn;b})+r^{b}_{nm}(r^{a}_{mn;c}+r^{c}_{mn;a})+r^{c}_{nm}(r^{a}_{mn;b}+r^{b}_{mn;a})]$$

where r is the position operator, $\hbar\omega_{nm} = \hbar\omega_n - \hbar\omega_m$ is the energy difference for the bands m and n, $f_{mn} = f_m - f_n$ is the difference of the Fermi distribution functions, subscripts a, b, and c are Cartesian indices, and $r^{b}_{mn;a}$ is the so-called generalized derivative of the coordinate operator in k space,

$$r^{b}_{nm;a} = \frac{r^{a}_{nm}\Delta^{b}_{mn}+r^{b}_{nm}\Delta^{a}_{mn}}{\omega_{nm}}+\frac{i}{\omega_{nm}}\times\sum_{l}(\omega_{lm}r^{a}_{nl}r^{b}_{lm}-\omega_{nl}r^{b}_{nl}r^{a}_{lm})$$

where $\Delta^{a}_{nm} = (p^{a}_{nn} - p^{a}_{mm}) / m$ is the difference between the electronic velocities at the bands n and m.

The $\chi^{(2)}$ coefficients here were calculated from PBE wavefunctions with a 7×7×3 k-point grid and about 168 bands. A scissor operator has been added to correct the conduction band energy (corrected to the experimental gap), which has been proved to be reliable in predicting the second order susceptibility for semiconductors and insulators.[20-22]

For an external radiation electric field E, the dipole moment μ_i of a group can be expressed as a Taylor series expansion[23-24]

$$\mu_i = \mu_i^0 + \alpha_{ij}E_j + \frac{1}{2!}\beta_{ijk}E_jE_k + \frac{1}{3!}\gamma_{ijkl}E_jE_kE_l$$

where i, j, k and l subscripts represent the different Cartesian coordinate components x, y, or z. μ_i^0 is the permanent dipole moment of a group, namely the dipole moment without an applied electric field. Physical quantities α, β, and γ correspond to the linear polarizability (α, which corresponds to the linear optical coefficient of a group), first-order hyperpolarizability tensor (β, which is the second-order nonlinear optical coefficient of a group), and second-order hyperpolarizability tensor (γ, which is the third-order nonlinear optical coefficient of a group), respectively.

We calculate the dipole moment, the static linear polarizability (α) and static first-order

hyperpolarizability (β) of [PbO_4I_2] and [$OOCCH_2COO$] groups at the PBE1PBE level[25] of theory with a reasonably large basis set def2TZVP[26-27] by using the Gaussian 09 program.[28] The polarizability anisotropy (Δα) was obtained by the formula (2) to reflect the source of birefringence.[29] The static first hyperpolarizability (β) was used to study the source of SHG response.

$$\Delta\alpha = \sqrt{\left[(\alpha_{xx} - \alpha_{yy})^2 + (\alpha_{xx} - \alpha_{zz})^2 + (\alpha_{yy} - \alpha_{zz})^2\right]/2}$$

2. Tables and Figures

Table S1. Crystal data and structure refinements for **KPMI** and **CPMI**.

Empirical formula	**$K_2I[PbI(OOCCH_2COO)]$**	**$Cs_2I_2[Pb(OOCCH_2COO)]$**
Formula weight	641.24	828.86
Temperature(K)	293(2)	293(2)
Crystal color	Colorless	Colorless
Wavelength(Å)	0.71073	0.71073
Crystal system	Orthorhombic	Orthorhombic
Space group	*Amm*2	*Pnma*
a / Å	6.038(5)	14.012(2)
b / Å	6.442(6)	6.6912(13)
c / Å	13.903(13)	13.4144(18)
Volume / Å^3	540.8(8)	1257.7(4)
Z	2	4
ρ_{calcd} / g·cm^{-3}	3.938	4.377
μ / mm^{-1}	22.052	24.007
F(000)	556.0	1400.0
Date / restraints / parameters	628/7/43	1562/0/65
2-Theta range for data collection	5.86 to 54.87	4.204 to 54.956
Limiting indices	$-7 \le h \le 7$, $-8 \le k \le 8$, $-13 \le l \le 18$	$-18 \le h \le 18$, $-8 \le k \le 8$, $-17 \le l \le 17$
Reflections collected / unique	2395/650 [R_{int} = 0.0574]	10962/1562 [R_{int} = 0.0769]
Completeness	99.0%	99.5%
Goodness-of-fit on F^2	1.054	1.072
R_1,wR_2 ($I > 2\sigma$) [a]	R_1=0.0424, R2=0.1001	R_1 = 0.0358, R_2 = 0.0819
R_1,wR_2 (all data)	R_1=0.0427, R2=0.1003	R_1 = 0.0419, R_2 = 0.0850
Largest diff ,peak and hole/ e·Å^{-3}	1.62 and -1.45	2.02 and -2.31

[a] $R_1 = \Sigma||F_o| - |F_c||/\Sigma|F_o|$ and $wR_2 = [\Sigma w(Fo^2 - Fc^2)^2/ \Sigma w F_o^4]^{1/2}$.

Table S2. Atomic coordinates, equivalent isotropic displacement parameters (Å^2) and BVS of **KPMI.**

Atom	*Wyck.*	*x*	*y*	*z*	U_{eq}[a]	BVS[b]
Pb1	2b	0.5000	1	0.56063(2)	0.0242(4)	1.72
I1	2a	0	1	0.6553(2)	0.0362(7)	-0.88
I2	2b	0.5000	0.5000	0.67446(19)	0.0320(8)	-0.64
K1	2a	0	0.5000	0.5251(8)	0.0292(17)	0.98
K2	2a	0	1	0.3356(7)	0.039(2)	0.77
O1	8f	0.3150(20)	0.7597(15)	0.4370(11)	0.031(3)	-2.16
C1	4e	0.5000	0.6920(30)	0.4079(16)	0.022(4)	
C2	2b	0.5000	0.5000	0.3410(30)	0.026(8)	

[a] U_{eq} is defined as 1/3 of the trace of the orthogonalised U_{ij} tensor.
[b] Bond valence sums were calculated by the equation：$s = \exp[(R_0 - R_i)/b]$, where R_0 and b are the bond valence parameters and R_i is the observed bond lengths.

Table S3. Atomic coordinates and equivalent isotropic displacement parameters (Å^2) for **CPMI**.

Atom	*Wyck.*	*x*	*y*	*z*	U_{eq}[a]
Pb1	4c	0.38225(3)	0.7500	0.37572(2)	0.02519(16)
Cs1	4c	0.13431(6)	0.7500	0.61390(5)	0.0329(2)
Cs2	4c	0.16570(5)	0.7500	0.13052(4)	0.02831(19)
I1	4c	0.49061(6)	0.7500	0.61127(5)	0.0321(2)
I2	4c	0.48843(6)	0.7500	0.14443(5)	0.0338(2)
O1	8d	0.2605(4)	0.5132(7)	0.4563(3)	0.0305(11)
O2	8d	0.2708(4)	0.5041(7)	0.2908(3)	0.0301(11)
C1	8d	0.2384(5)	0.4355(10)	0.3732(4)	0.0224(13)
C2	4c	0.1741(8)	0.2500	0.3709(7)	0.029(2)

[a]U_{eq} is defined as 1/3 of the trace of the orthogonalised U_{ij} tensor.

.

Table S4. Anisotropic displacement parameters (Å^2) of **KPMI**.

Atom	**U_{11}**	**U_{22}**	**U_{33}**	**U_{23}**	**U_{13}**	**U_{12}**
Pb1	0.0195(6)	0.0266(6)	0.0267(6)	0.0000	0.0000	0.0000
I1	0.0212(15)	0.0469(16)	0.0404(15)	0.0000	0.0000	0.0000
I2	0.0325(17)	0.0327(14)	0.0308(14)	0.0000	0.0000	0.0000
K1	0.017(4)	0.024(3)	0.046(4)	0.0000	0.0000	0.0000
K2	0.030(5)	0.044(4)	0.043(5)	0.0000	0.0000	0.0000
O1	0.030(7)	0.023(5)	0.038(7)	-0.002(5)	0.0010(6)	0.0040(4)
C1	0.021(4)	0.022(4)	0.022(4)	0.0004(13)	0.0000	0.0000
C2	0.024(18)	0.015(12)	0.040(20)	0.0000	0.0000	0.000

Table S5. Anisotropic displacement parameters (Å^2) of **CPMI.**

Atom	**U_{11}**	**U_{22}**	**U_{33}**	**U_{23}**	**U_{13}**	**U_{12}**
Pb1	0.0258(2)	0.0244(3)	0.0253(2)	0.0000	-0.00098(12)	0.0000
Cs1	0.0453(4)	0.0246(4)	0.0286(3)	0.0000	0.0007(3)	0.0000
Cs2	0.0339(4)	0.0281(4)	0.0229(3)	0.0000	-0.0017(2)	0.0000
I1	0.0391(4)	0.0288(4)	0.0283(4)	0.0000	0.0017(2)	0.0000
I2	0.0405(4)	0.0316(4)	0.0294(3)	0.0000	0.0007(3)	0.0000
O1	0.037(3)	0.026(3)	0.028(3)	-0.005(2)	0.0005(19)	0.0000(2)
O2	0.037(3)	0.028(3)	0.025 (2)	0.002(2)	0.0008(19)	-0.0002(2)
C1	0.024(3)	0.017(3)	0.027(3)	0.001(2)	-0.002(2)	0.0008(3)
C2	0.031(6)	0.025(6)	0.031(6)	0.0000	-0.008(4)	0.0000

Symmetry transformations used to generate equivalent atoms: #1 1-x, +y, +z; #2+x, 2-y, +z; #3 1-x, 2-y, +z; #4 1+x, +y, +z

Table S6. Selected bond lengths (**Å**) and angles (deg.) for **CPMI**.

Pb(1)-O(1)	2.567(5)	Pb(1)-O(2)	2.538(5)
Pb(1)-O(1)$^{\#1}$	2.567(5)	Pb(1)-O(2)$^{\#1}$	2.538(5)
O(1)-Pb(1)-O(1)$^{\#1}$	76.2(2)	O(1)$^{\#1}$-Pb(1)- O(2)	100.39(17)
O(1)-Pb(1)-O(2)	51.69(16)	O(1)$^{\#1}$-Pb(1)-O(2)$^{\#1}$	51.69(16)
O(1) -Pb(1)- O(2)$^{\#1}$	100.39(17)	O(2)-Pb(1)-O(2)$^{\#1}$	73.4(5)

Symmetry transformation used to generate equivalent atoms: #1 +x, 3/2-y, +z;

Table S7. Selected bond lengths (**Å**) and angles (deg.) for **KPMI**.

Pb(1)-O(1)	2.570(13)	Pb(1)-O(1)$^{\#3}$	2.570(13)
Pb(1)-O(1)$^{\#1}$	2.570(13)	Pb(1)-I(1)	3.293(3)
Pb(1)-O(1)$^{\#2}$	2.570(13)	Pb(1)-I(1)$^{\#4}$	3.293(3)
O(1)-Pb(1)-O(1)$^{\#1}$	51.6(6)	O(1)$^{\#1}$-Pb(1)- I(1)$^{\#4}$	82.4(3)
O(1)-Pb(1)-O(1)$^{\#2}$	96.1(6)	O(1)$^{\#2}$-Pb(1)-O(1)$^{\#3}$	51.6(6)
O(1)-Pb(1)-O(1)$^{\#3}$	74.1(5)	O(1)$^{\#2}$-Pb(1)-I(1)	131.4(3)
O(1)-Pb(1)-I(1)	131.8(3)	O(1)$^{\#2}$-Pb(1)-I(1)$^{\#4}$	82.4(3)
O(1)-Pb(1)-I(1)$^{\#4}$	131.8(3)	O(1)$^{\#3}$-Pb(1)-I(1)	82.4(3)
O(1)$^{\#1}$-Pb(1)-O(1)$^{\#2}$	74.1(5)	O(1)$^{\#3}$-Pb(1)-I(1)$^{\#4}$	131.8(3)
O(1)$^{\#1}$-Pb(1)-O(1)$^{\#3}$	96.1(6)	I(1)-Pb(1)-I(1)$^{\#4}$	132.89(11)
O(1)$^{\#1}$-Pb(1)-I(1)	131.8(3)		

Symmetry transformations used to generate equivalent atoms: #1 1-x, +y, +z; #2+x, 2-y, +z; #3 1-x, 2-y, +z; #4 1+x, +y, +z.

Table S8 The SHG responses and thermal stabilities of malonates.

Crystal Name	Space Group	SHG response	Thermal stability	Birefringence	References
bis(2-aminopyridinium) malonate	*Fdd2*	4.2 × KDP	101.7 °C	*	**[30]**
2-methylimidazolium malonate	$P2_1$	1.24 × KDP	154 °C	*	**[31]**
$MnC_3H_2O_4·2H_2O$	$Pca2_1$	0.7 × KDP	127 °C	*	**[32]**
$C_9H_{11}NO_2·C_9H_{12}NO_2^+·C_3H_3O_4^-$	$P2_1cn$	0.38 × KDP	184.5 °C	*	**[33]**
L-Histidine malonate	*	0.76 × KDP	72 °C	*	**[34]**
$Co[CS(NH_2)_2]_2·C_3H_2O_4·2H_2O$	*	0.41 × KDP	120.13 °C	*	**[35]**
$Ni[CS(NH_2)_2]_2·C_3H_2O_4·2H_2O$	*	0.35 × KDP	126.16 °C	*	**[35]**
$[3H_2O(C_3H_2O_4)_3Ce_2]·2H_2O$	$P2_1$	1 × KDP	100 °C	*	**[36]**
$KLi(C_3H_2O_4)·H_2O$	$Pna2_1$	3 × KDP	120 °C	0.103@1064 nm(*Cal.*)	**[37]**
$K_2Pb[OOCCH_2COO]I_2$	***Amm*2**	**6.3 × KDP**	**200 °C**	**0.218@546 nm(*Obv.*)**	**This work**

***** is not mentioned in the original article.

Table S9. The local dipole moment (μ) in Debye, polarizability anisotropy ($\Delta\alpha$), and first hyperpolarizability (β) in 10^{-30} esu for two [PbO_4I_2] polyhedrons and two [$OOCCH_2COO$] groups in per unit cell of **KPMI**. The charge of the structural group was estimated by the Bader charge of each atom.

Dipole moment	**x**	**y**	**z**	**$\Delta\alpha$**	**β (10^{-30} esu)**
[PbO_4I_2]	0.000	0.000	18.181	26.431	619.2367
[PbO_4I_2]	0.000	0.000	18.181	26.431	619.2367
[$OOCCH_2COO$]	0.000	0.000	-3.705	2.250	-2.419
[$OOCCH_2COO$]	0.000	0.000	-3.705	2.250	-2.419
Total (D)	0	0	28.952		

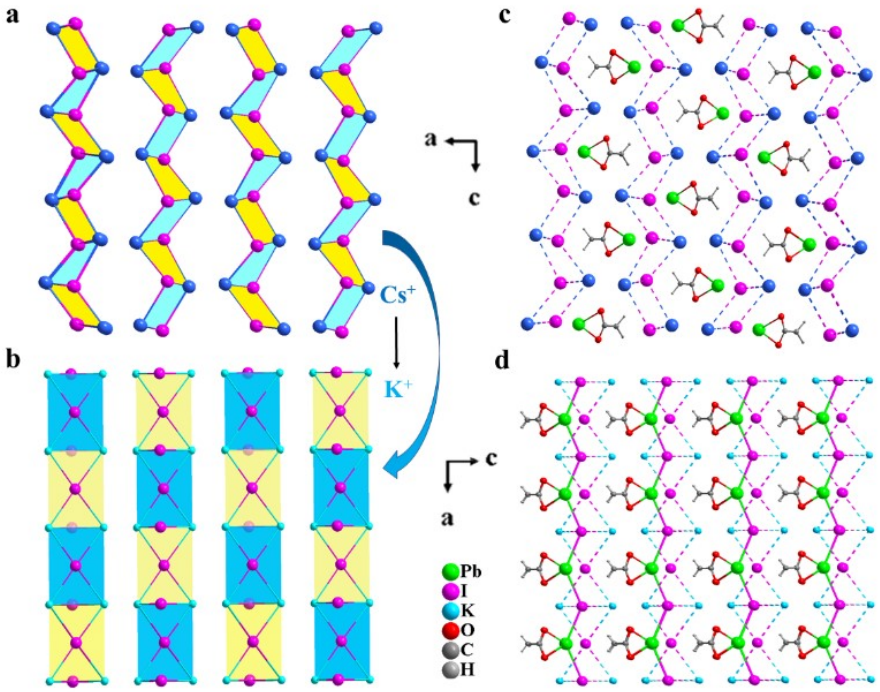

Fig. S1. (a) The wave-like [CsI] inorganic layers in **CPMI**. (b) The 2D [K_2I] inorganic frameworks in **KPMI**. Ball-stick views of (c) **CPMI** and (d) **KPMI**.

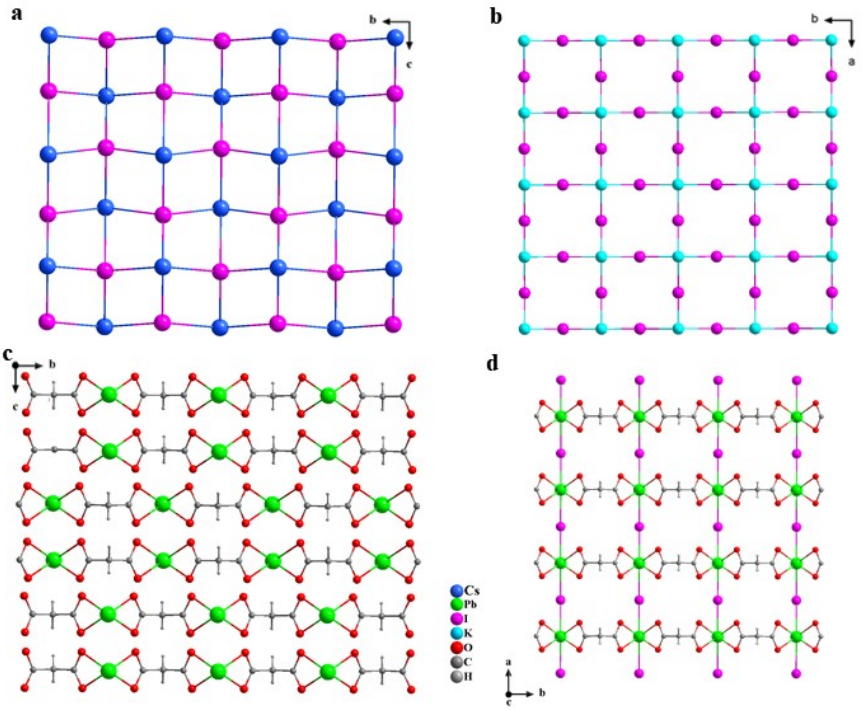

Fig. S2. (a) The wave-like [CsI] inorganic layer in **CPMI**. (b) The 2D [K_2I] inorganic framework in **KPMI**; (c) The [PbM] chains in **CPMI**. (d) The [$PbMI_2$] layer in **KPMI**.

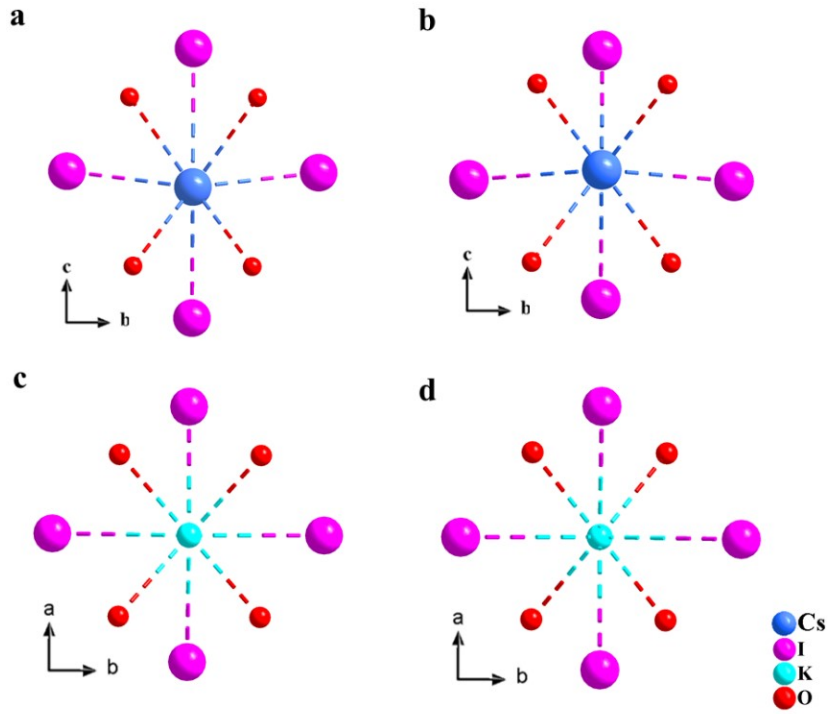

Fig. S3. The environments of (a) $Cs1^+$ and (b) $Cs2^+$ cations in **CPMI**. The environments of (c) $K1^+$ and (d) $K2^+$ cations in **KPMI**.

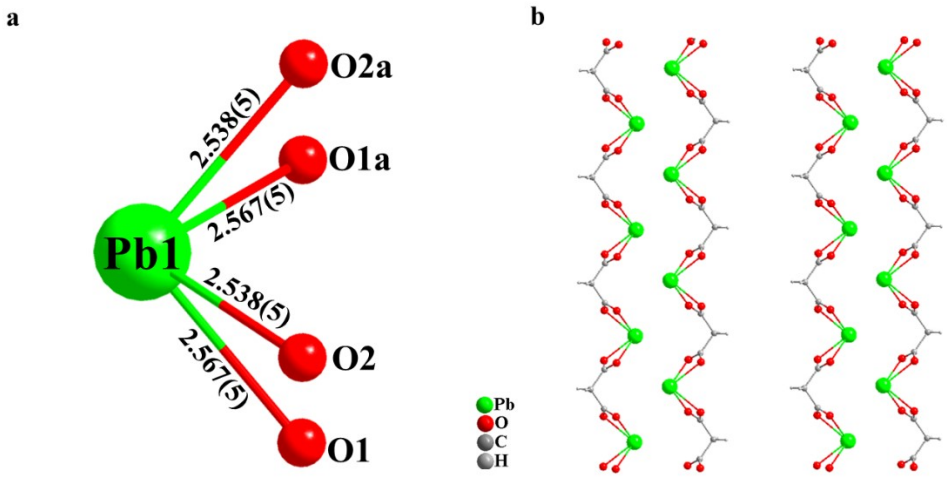

Fig. S4. Ball-stick views of (a) the coordination environment of the Pb(II) atom and [PbM] chains in **CPMI**. Symmetry code: a 1+x, 3/2-y, +z.

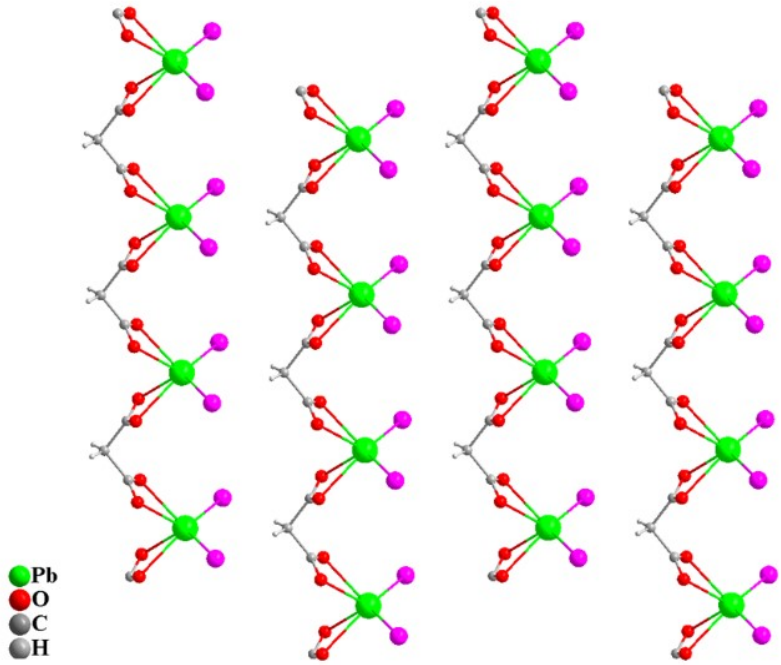

Fig. S5. A ball-stick view of [PbM] chains in **KPMI**.

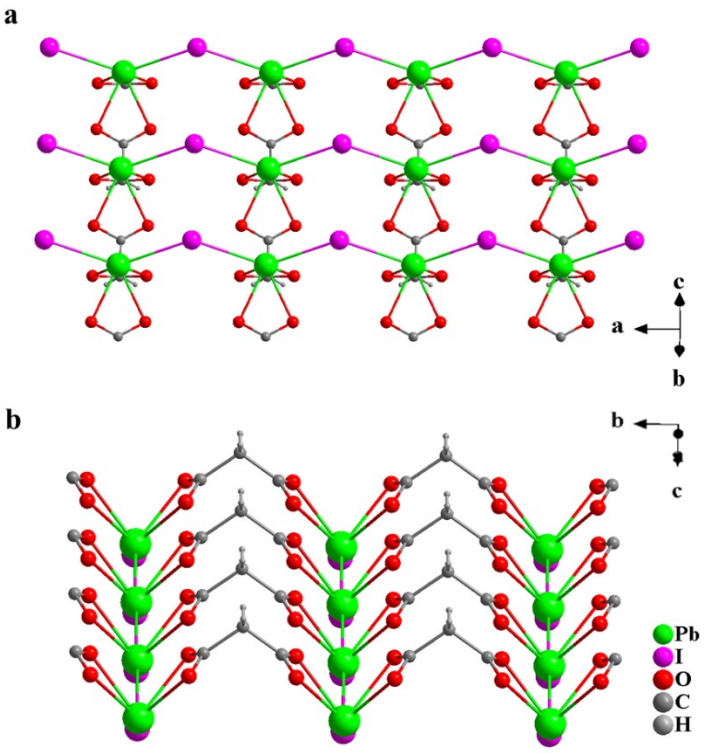

Fig. S6. (a) The [$PbMI_2$] layer along the *a* axis. (b) The [$PbMI_2$] layer along the *b* axis.

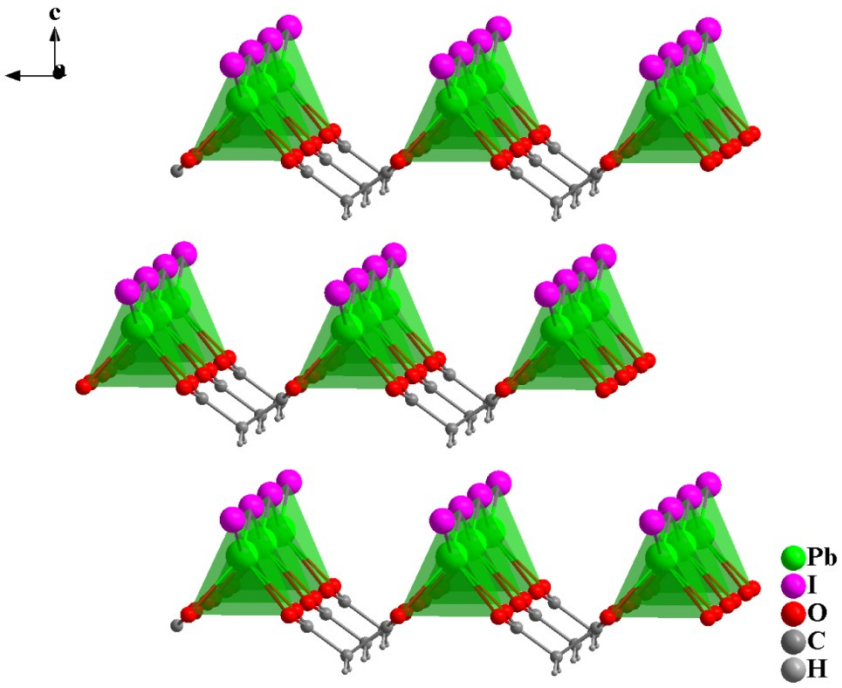

Fig. S7. The oriented arrangement of [$PbMI_2$] layers in **KPMI**.

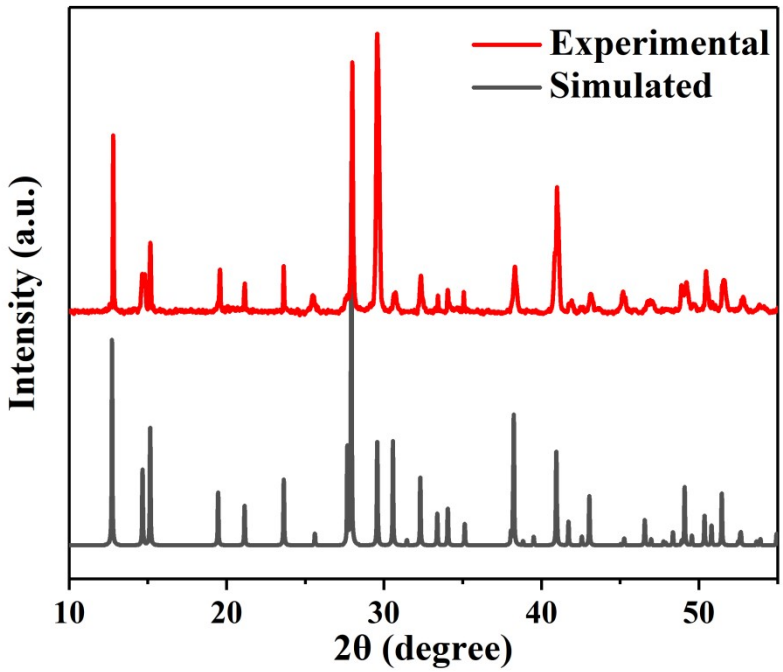

Fig. S8. Experimental and simulated PXRD patterns of **KPMI**.

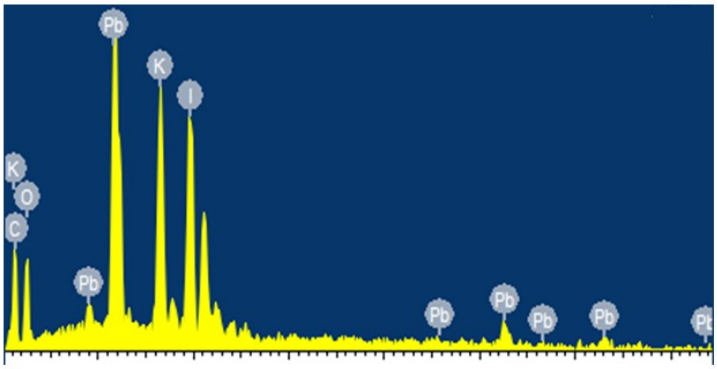

Fig. S9. The EDS spectrum of **KPMI**.

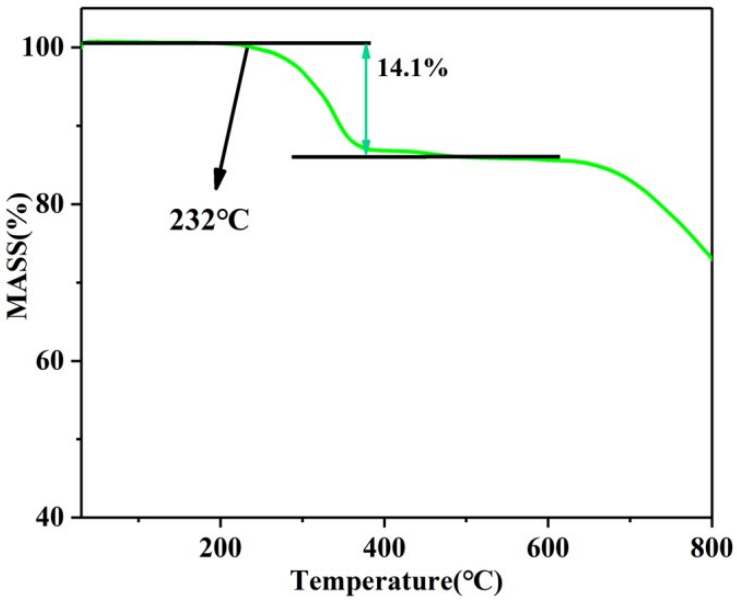

Fig. S10. The TGA curve of **KPMI**.

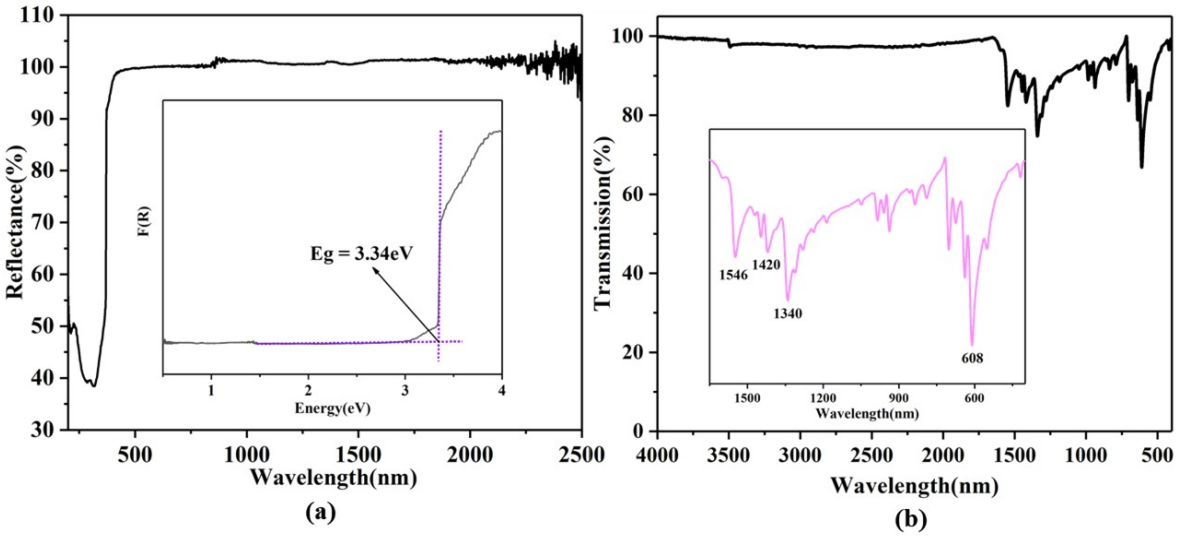

Fig. S11. The UV-vis–NIR and IR spectra of **KPMI**.

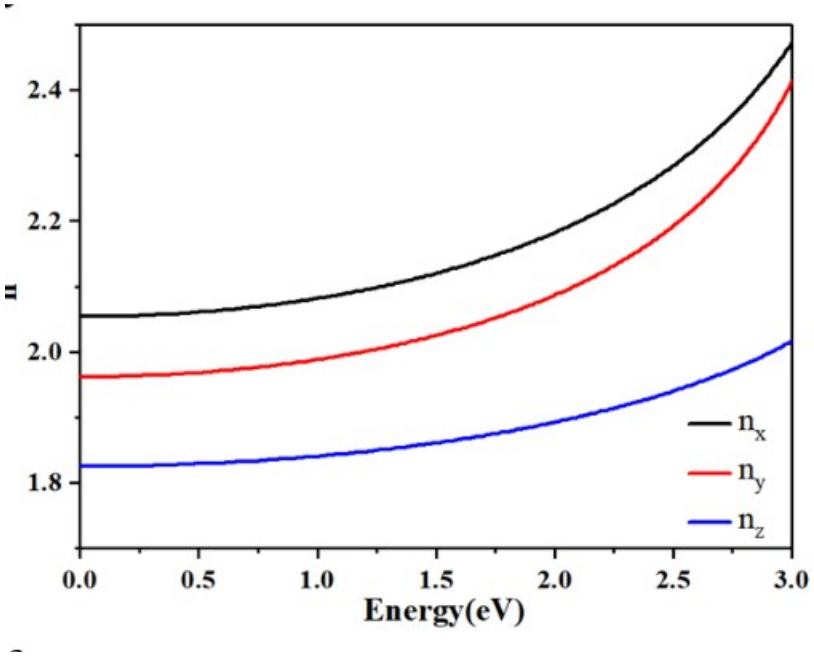

Fig. S12. The refractive index dispersion curves of **KPMI**..

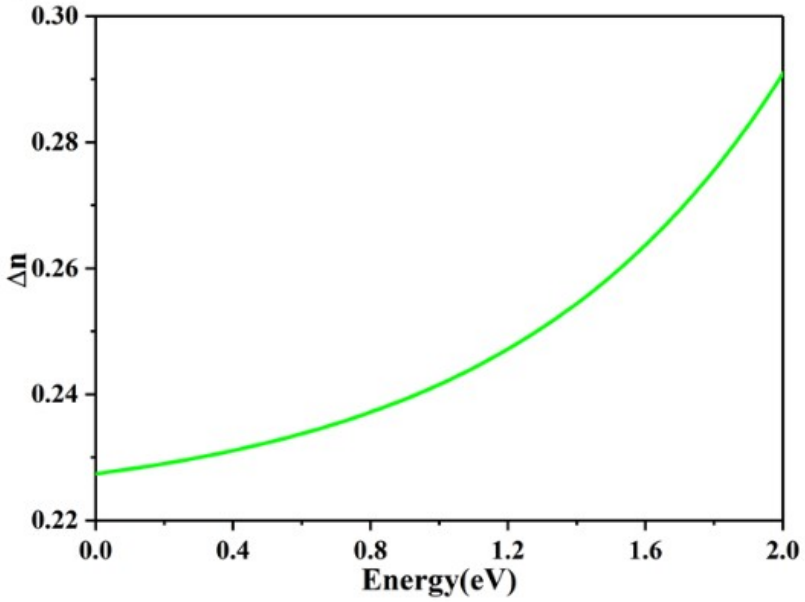

Fig. S13. The calculated birefringence curve of **KPMI**..

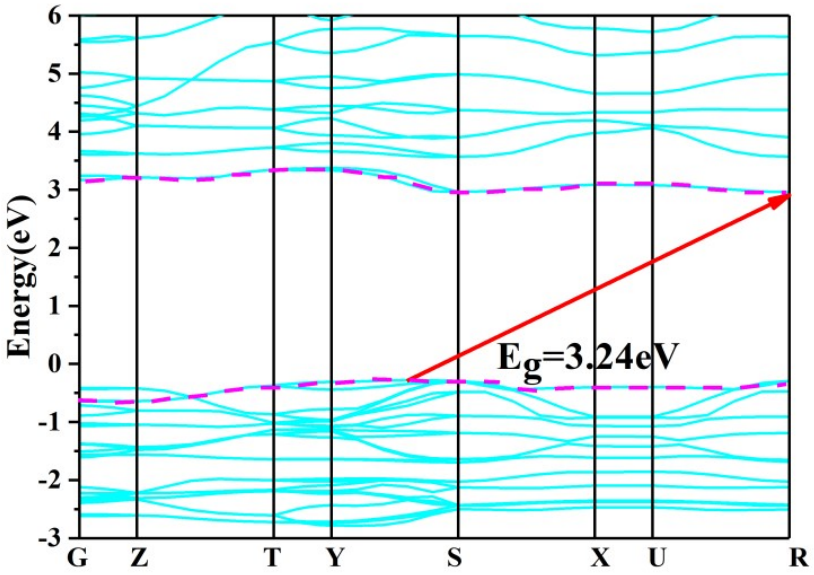

Fig. S14. The calculated band structure of **KPMI**.

3. References

[1] G. M. Sheldrick, *Acta Crystallogr. A* 2015, **71**, 3-8.

[2] G. M. Sheldrick, *Acta crystallogr. Sect. C: Struct. Chem.* 2015, **71**, 3-8.

[3] A. Spek, *J. appl. Crystallogr.* 2003, **36**, 7-13.

[4] P. Kubelka, F. Munk, *Z. Tech. Phys.* 1931, **12**, 259-274.

[5] S. Kurtz, T. Perry, *J. Appl. Phys*. 1968, **39**, 3798-3813.

[6] G. Kresse, Vienna ab Initio Simulation Package (VASP).

[7] G. Kresse, J. Furthmüller, *Phys. Rev. B* 1996, **54**, 11169-11186

[8] G. Kresse, D. Joubert, *Phys. Rev. B* 1999, **59**, 1758-1775.

[9] J. P. Perdew, K. Burke, M. Ernzerhof, *Phys. Rev. Lett.* 1996, **77**, 3865-3868.

[10] P. Bliichl, *Phys. Rev. B* 1994, **50**, 17953-17979.

[11] H. J. Monkhorst, J. D. Pack, *Phys. Rev. B* 1976, **13**, 5188-5192.

[12] Hongzhiwei Technology, Device Studio, Version 2021A. *China*, 2021. Available online: https: //iresearch.net.cn/cloudSoftware.

[13] K. Momma, F. Izumi, *J. Appl. Crystallogr.* 2011, **44**, 1272-1276.

[14] C. Aversa, J. Sipe, *Phys. Rev. B* 1995, **52**, 14636-14645

[15] S. N. Rashkeev, W. R. Lambrecht, B. Segall, *Phys. Rev. B* 1998, **57**, 3905-3919.

[16] J. Hu, Z. Ma, J. Li, C. He, Q. Li, K. Wu, *J. Phys. D: Appl. Phys.* 2016, **49**, 185103.

[17] J. Li, Z. Ma, C. He, Q. Li, K. Wu, *J. Mater. Chem. C* 2016, **4**, 1926-1934.

[18] Z. Ma, K. Wu, R. Sa, K. Ding, Q. Li, *AIP. Adv.* 201**2**, **2**, 032170.

[19] Z. Ma, K. Wu, R. Sa, Q. Li, Y. Zhang, *J. Alloy. Compd.* 2013, **568**, 16-20.

[20] B. Champagne, D. M. Bishop, *Adv. Chem. Phys.* 2003, **126**, 41-92.

[21] A. H. Reshak, S. Auluck, I. Kityk, *Phys. Rev. B* 2007, **75**, 245120.

[22] Y.-Z. Huang, L.-M. Wu, X.-T. Wu, L.-H. Li, L. Chen, Y.-F. Zhang, *J. Am. Chem. Soc.* 2010, **132**, 12788-12789.

[23] J. E. Rice, R. D. Amos, S. M. Colwell, N. C. Handy, J. Sanz, *J. Chem. Phys.* 1990, **93**, 8828-8839.

[24] Y. C. Yang, X. Liu, J. Lu, L. M. Wu, L. Chen, *Angew. Chem. Int. Ed.* 2021, **60**, 21216-21220.

[25] P. E. Blöchl, *Phys. Rev. B* 1994, **50**, 17953-17979.

[26] F. Weigend, R. Ahlrichs, *Phys. Chem. Chem. Phys.* 2005, **7**, 3297-3305.3

[27] F. Weigend, *Phys. Chem. Chem Phys.* 2006, **8**, 1057-1065.

[28] T. Lu, F. Chen, *J. Comput. Chem.* 2012, **33**, 580-592.

[29] Gaussian 09, Revision A.02, M. J. Frisch, G. W. *et al.* Gaussian, Inc., Wallingford CT, 2016.

[30] R. Chitra, R. Choudhury, V. Thiruvenkatam, M. Hosur, T. G. Row, *J. Mol. Struct.* 2012, **1010**, 46-51.

[31] K. Elangovan, A. Senthil, *J. Mater. Sci: Mater. Electron.* 2019, **30**, 14143-14150.

[32] A. Lincy, V. Mahalakshmi, J. Thomas, K. Saban, *Opt.* 2013, **124**, 2881-2884.

[33] K. Sangeetha, S. Rajina, M. Marchewka, J. Binoy, *Mater. Today: Proceedings* 2020, **25**, 307-315.

[34] K. Ramya, N. Saraswathi, C. R. Raja, *Optics & Laser Technology* 2016, **84**, 102-106.

[35] N. M. Raste, K. S. Pardeshi, *J. Opt. Adv. Mater.* 2016, **18**, 445-452.

[36] A. Lincy, V. Mahalakshmi, J. Thomas, P. Raghavaiah, K. Saban, *Optik* 2016, **127**, 2197-2201.

[37] L. Cao, H. Tian, D. Lin, C. Lin, F. Xu, Y. Han, T. Yan, J. Chen, B.-X. Li, N. Ye, *Chem. Sci.* 2022.